G.S. Mityurich[1], P. Ranachowski[2], E.V. Lebedeva[3], M. Aleksiejuk[2], A.N. Serdyukov[1]
[1]Francisk Skorina Gomel State University, Gomel, Belarus
[2]Institute of Fundamental Techmological Reasearch PAS, Warsaw, Poland
[3]Belarusian Trade and Economics University of Consumer Cooperatives, Gomel, Belarus

PIEZOELECTRIC DETECTION OF PHOTOACOUSTIC SIGNAL IN DENCE LAYER OF CARBON NANOTUBES IRRADIATED BY BESSEL LIGHT BEAMS

Introduction

Bessel light beams (BLB) are used and widely used in laser photoacoustic methods to diagnose the structure of various samples as a source of sound excitation [1-4]. In particular, the use of Bessel light beams in optical-acoustic microscopy makes it possible to effectively increase the focal depth of the resulting photoacoustic image in comparison with a conventional Gaussian light beam. The use of different types of BLB polarization modes is explained by the fact that BLBs have a number of unique properties, for example, non-diffraction of propagation in space.

Promising material in various fields of science and technology are carbon nanotubes (CNTs). One of the main advantages of these structures is the ability to control the properties of the created CNT layers (Figure 1) by changing the geometric dimensions and configuration of nanoobjects.

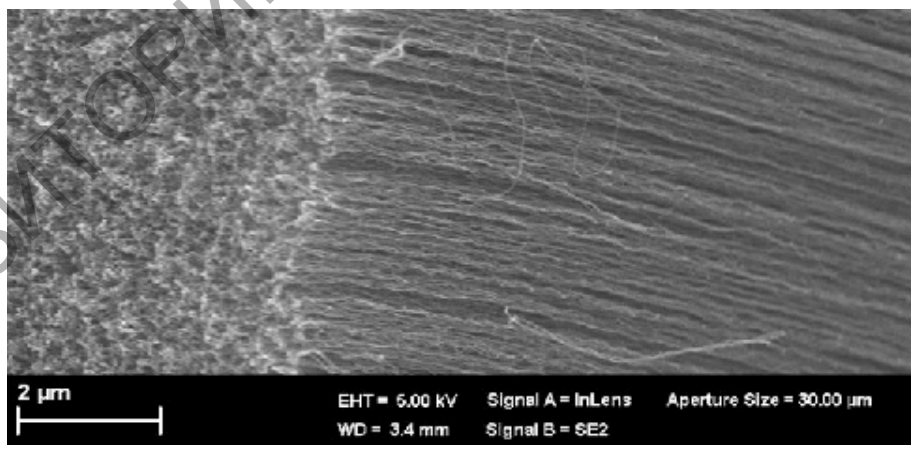

Figure 1 – Cross-section of a CNT array (Focussed ion beam scanning electron microscope, Zeiss–Neon 40 EsB) [5]

The classical theory of electrodynamics can not always be applied to the description of nanotubes. Consequently, it is required to search for new quasiclassical theoretical approaches and studies that would enable us to solve the problems of micro- and macroscopic electrodynamics [6], which underlie the theoretical basis of modern photoacoustic spectroscopy.

This paper is devoted to the construction of a model of photoacoustic conversion of BLB modes in a layer of chiral and achiral carbon nanotubes for the case of piezoelectric recording of the resultant signal.

1. Conductivity of chiral and axiral carbon nanotubes

By analogy with [6], the conductivity of chiral CNTs in cylindrical coordinates is determined by the relation, (electron velocity $v_e << c$, c – speed of light)

$$\sigma_{zz}(\omega) = -\frac{2P_0 ie^2}{\pi\hbar\sqrt{n^2+nm+m^2}}\frac{1}{(\omega+i\nu)}\sum_{s=1}^{m}\upsilon_z^2(p_z,s)\frac{\partial F}{\partial\varepsilon}, \qquad (1)$$

where the expression for the velocity projection

$$\upsilon(p_z) = \pm\frac{\sqrt{3}\gamma_0 a}{\hbar\sqrt{n^2+nm+m^2}}[m\sin(\psi_1-\psi_2)-$$
$$-n\sin(\psi_1+\psi_2)-(n+m)\sin 2\psi_2]/(1+4\cos\psi_1\cos\psi_2+4\cos^2\psi_2),$$

$$\psi_1(p_z) = \frac{1}{\sqrt{n^2+nm+m^2}}\left(\frac{3\pi q(n+m)}{2\sqrt{n^2+nm+m^2}}+\frac{\sqrt{3}ap_z(n-m)}{4\hbar}\right),$$

$$\psi_1(p_z) = \frac{1}{\sqrt{n^2+nm+m^2}}\left(\frac{\pi q(n-m)}{2\sqrt{n^2+nm+m^2}}+\frac{\sqrt{3}ap_z(n+m)}{4\hbar}\right)$$

For CNTs of the zigzag type, the expressions for the axial conductivity are expressed by the formula

$$|\sigma_{zz}(\omega)| = \frac{2w_{cn}e^2P_0}{\sqrt{3}\pi^2R_{cn}\sqrt{(\omega^2+\nu^2)}k_BT}\sum_{S=1}^{m}\frac{\exp(\varepsilon_0/k_BT)}{[1+\exp(\varepsilon_0/k_BT)]^2},$$

$$\varepsilon_0 = \varepsilon(P_0) = \gamma\sqrt{1+4\cos(aP_0)\cos\left(\frac{\pi S}{m}\right)+4\cos^2\left(\frac{\pi S}{m}\right)}.$$

Also obtained expression describing the axial conductivity in carbon nanotubes armchair type

$$|\sigma_{zz}(\omega)| = \frac{2w_{cn}e^2P_0}{\pi^2R_{cn}\sqrt{(\omega^2+\nu^2)}k_BT}\sum_{S=1}^{m}\frac{\exp(\varepsilon_0/k_BT)}{[1+\exp(\varepsilon_0/k_BT)]^2},$$

$$\varepsilon_0 = \varepsilon(P_0) = \gamma\sqrt{1+4\cos\left(\frac{a\hbar S}{R_0}\right)\cos\left(\frac{aP_0}{\sqrt{3}}\right)+4\cos^2\left(\frac{aP_0}{\sqrt{3}}\right)}.$$

The expression for the projection of the electron velocity vector on the z axis is obtained with allowance for the formula $\upsilon(p_z) = \partial\varepsilon(\mathbf{p})/\partial p_z$ [7] and the relationship for the energy distribution within the tight-binding approximation, which takes into account the interaction of only the nearest neighboring atoms in the hexagonal structure [8, 9].

2. Dissipation of energy of Bessel light beamesiIn chiral and achiral carbon nanotubes

The effect of a Bessel light beam on the absorbing layer of chiral nanotubes leads to a periodic change in the temperature field, which can be described by the equation of thermal conductivity

$$\nabla^2 T - \frac{1}{\beta_S}\frac{\partial T}{\partial t} = -\frac{1}{2k_S}Q\left(1+e^{i\Omega t}\right), \qquad (2)$$

where $\beta_s = k_S/\rho_0 \cdot C$ is effective coefficient of thermal diffusivity, k_S is coefficient of thermal conductivity, ρ_0 is density of a layer of carbon nanotubes, C is specific heat of a layer of CNTs, Ω is modulation frequency.

In equation (2) Q is volume density of thermal sources, which is determined by the expression

$$Q = \sigma_{cn}|E|^2, \qquad (3)$$

where $|\sigma_{cn}| = 2\pi\cdot|\sigma_{zz}|/\lambda$ is conductivity of the CNT layer. Substituting into (3) the relation describing the intensity of the wave, it is easy to obtain the energy dissipation rate

$$Q = 2\alpha_0 I_0 e^{-2\alpha_{eff} z} = 2\sigma_{cn}/(c\sqrt{\varepsilon'}\varepsilon_0) I_0 e^{-2\alpha_{eff} z}. \qquad (4)$$

In the formula (4) I_0 is Proceeding from the geometry of chiral and achiral carbon nanotubes, it is expedient to write equation (2) in a cylindrical coordinate system. The absorption coefficient in (3) is defined as follows

$$\alpha_0 = (\omega/c)\cdot\left(\varepsilon''/\sqrt{\varepsilon'}\right) = (\omega/c)\cdot(\varepsilon''/n).$$

Conductivity is related to the imaginary part of the dielectric constant by the formula $\varepsilon = \varepsilon' + i\varepsilon''$, $\varepsilon'' = 4\pi\cdot\sigma/\omega$.

Thus, in cylindrical coordinates, the energy dissipation rate of Bessel light beams (BLB) in the layer of absorbing carbon chiral nanotubes can be represented as follows

$$Q^{TE} = \frac{2|\sigma_{cn}|I_0}{c\sqrt{\varepsilon'}\varepsilon_0}\frac{c}{4\pi}k_0\varepsilon_\alpha\left(n_1^2+n_2^2\right)\left[\frac{m^2}{(q\rho)^2}J_m^2(qr)+J_m'^2(qr)\right]\exp(-\alpha_{eff}z), \quad (5)$$

where $\alpha = 2k_{zz}$.

3. Calculation of the resulting photoacoustic signal

Let us determine the amplitude of the photoacoustic signal arising in the layer of chiral CNTs upon irradiation by the TE mode of the BLB, based on the use of the piezoelectric method of recording the signal in accordance with the scheme shown in figure 2.

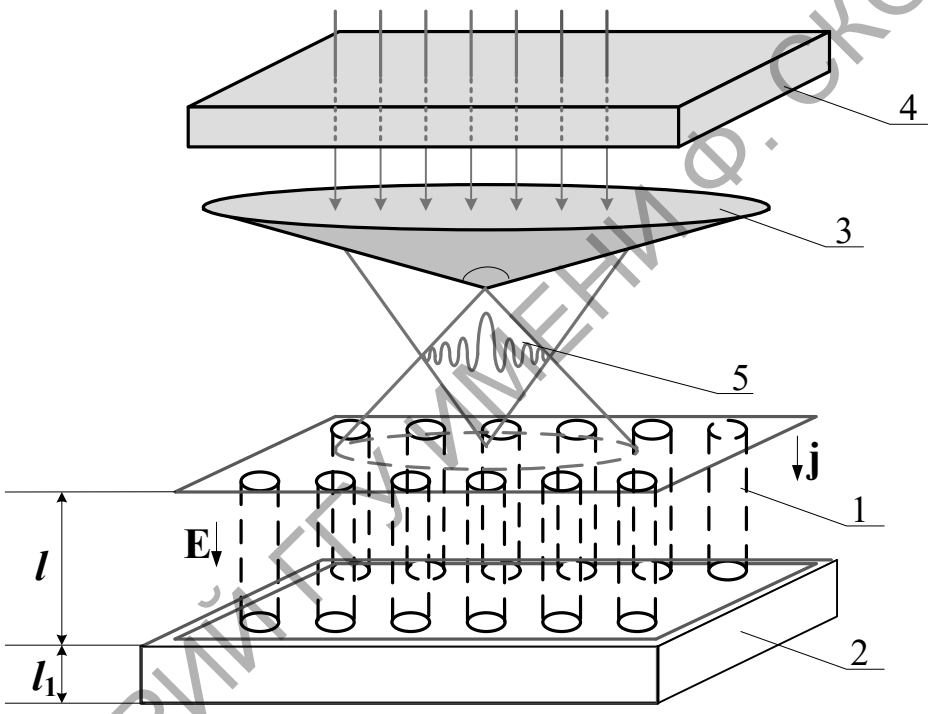

Figure 2 – The scheme of registration of a photoacoustic signal:
1 – the layer of chiral or achiral CNTs; 2 – piezoelectric detector; 3 – axicon;
4 – modulator; 5 – Bessel light beam

The simultaneous solution of the heat equation (2) and the equations for thermoelastic deformations in the sample and piezoelectric transducer l_1 allows us to find an expression for the photoacoustic signal.

Assuming the boundaries of the "sample-piezoelectric detector" system to be free ($\sigma(l=0)=0$, $\sigma(l_1=0)=0$) and also using the technique described in [10], we will find the expression for the no-load voltage V^{TE} on a piezo transducer

$$V^{TE} = \frac{e}{\varepsilon^S}\left(U_P\big|_{z=l_1} - U_P\big|_{z=0}\right) = \frac{e}{\varepsilon^S}Z\,R^{TE}. \quad (6)$$

In relation (5), the factor Z

$$Z = \frac{\sin^2\left(k_1 \Delta l / 2\right)}{m_0 \sin k_1 \Delta l \cos kl + \cos k_1 \Delta l \sin kl} \tag{7}$$

describes the purely acoustic properties of the "carbon nanotube-piezoelectric detector" system, and the factor R^{TE}

$$R^{TE} = \frac{\overline{E}^{TE} B_0 k}{\left(\lambda_l + 2\mu_l\right) k_S \sigma_S^2 \alpha_{ef}} \left[\frac{1 + \mu_1 + \mu_2^2 + \mu_3^2}{\left(1 + \mu_1\right) \cdot \left(1 + \mu_2^2\right) \cdot \left(1 + \mu_3^2\right)} \right] \tag{8}$$

determines the dissipative, dielectric, thermophysical, and thermoelastic properties of the sample under study, as well as the polarization and energy parameters of the BLB.

In the expressions (5)–(7) he following notation is introduced: $U(z)$, $U_p(z)$ are elastic displacements in the CNT layer and piezoelectric transducer; υ_{cn}, υ_p are values of velocities of elastic longitudinal waves, B_0 is the bulk modulus, $c^T = \lambda_l + 2/3\ \mu_l$, λ_l, μ_l are the Lame coefficients, a_0 is coefficient of volumetric thermal expansion, σ – values of elastic stresses, $\sigma_S = (1 - i)a_S$, $a_S = (\Omega/2\beta_{cn})^{1/2}$ is effective coefficient of thermal diffusion of the sample, β_{cn} is effective coefficient of sample thermal diffusivity, $\mu_1 = \alpha_{eff}/\sigma_S$, $\mu_2 = k/\sigma_S$, $\mu_3 = k/\alpha_{eff}$, $k_1 = \Omega/\upsilon_p$ is wave number of an elastic wave in a piezoelectric transducer, $k = \Omega/\upsilon_{cn}$ is wave number of a sound wave in a sample, $m_0 = (k_1 c^D)/(kc^T)$, $c^D = c^E\,(1 + e^2/\varepsilon^S c^E)$, c^E is coefficient of rigidity of a piezoelectric, e – piezoelectric module, ε^S – dielectric constant of a piezoelectric crystal,

$$\overline{E}^{TE} = \eta\, a_t\, \alpha_{ef}\, E^{TE}, \quad E^{TE} = A^{TE} \Big/ \left(\alpha_{ef}^2 - \sigma_S^2\right),$$

$$A^{TE} = \frac{2\left|\sigma_{cn}\right| I_0}{c\sqrt{\varepsilon'}\varepsilon_0} \frac{c}{4\pi} k_0 \varepsilon_\alpha \left(n_1^2 + n_2^2\right) \left[\frac{m^2}{(q\rho)^2} J_m^2(qr) + J_m'^2(qr) \right],$$

$J_m'(q\rho) = \partial J_m(q\rho)/\partial\,\rho$ is derivative of the Bessel function J_m(q ρ) from the radial coordinate ρ. Analysis of expression (6) for the amplitude of the photoacoustic signal showed the presence of resonant peaks in the region of gigahertz frequencies (Figures 3, 4).

We note that we have considered a particular case of the free boundaries of the "sample-piezotransducer" system. In this case, the potential difference recorded by the detector is determined by the formulas (6)–(8). When the boundary conditions change, the relationships for calculating the potential difference appearing in the detector will change. Under conditions where the boundaries of the "sample-piezoelectric detector" system are fixed ($U(0) = 0$, $U(l + l_1) = 0$) or alternately loaded ($\sigma(0) = 0$,

$U(l + l_1) = 0$; $\sigma(l + l_1) = 0$ $U(0) = 0$), other expressions for the potential difference are obtained. However, even in these particular situations, the main regularities of the photoacoustic transformation of the TE-mode of the BLB in magnetically low-dimensional structures correspond to those revealed on the basis of the model of free boundaries.

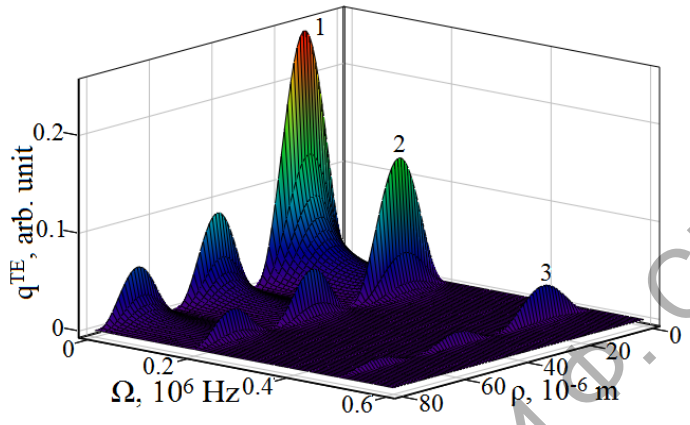

Figure 3 – Dependence of the amplitude of the PA signal on the radial coordinate and modulation frequency of the BLB (m = 0, α = 1°)

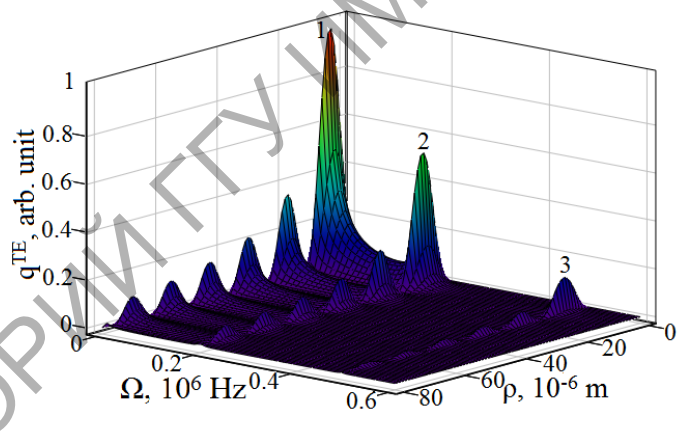

Figure 4 – Dependence of the amplitude of the PA signal on the radial coordinate and modulation frequency of the BLB (m = 0, α = 2°)

Using expression (6) for the idling voltage, it is possible to determine the amplitudes of photoacoustic signals for the system "sample-piezoelectric transducer" with alternately loaded boundaries:

$$\begin{cases} \sigma(l) = \sigma_p(l), \\ U(l) = U_p(l), \\ \sigma(0) = 0, \\ U_p(l_1) = 0, \end{cases} \qquad (9)$$

$$\begin{cases} \sigma(l) = \sigma_p(l), \\ U(l) = U_p(l), \\ \sigma_p(l_1) = 0, \\ U(0) = 0. \end{cases} \tag{10}$$

The difference in the amplitude of the displacement of the boundaries of the system when the boundary conditions (9) is realized is determined by the following relation

$$U^{TE} = \frac{A_1' C_2' - A_2' C_1'}{A_1' B'_2 + A_2' B'_1} \left(e^{-2ik_1 l_1} e^{ik_1 l} - e^{-ik_1 l} \right), \tag{11}$$

where

$$A_1' = 2k c^T \sin kl; \; A_2' = 2\cos kl;$$

$$B_1' = ik_1 c^D \left(e^{-2ik_1 l_1} e^{ik_1 l} + e^{-ik_1 l} \right); \; B_2' = \left(e^{-2ik_1 l_1} e^{ik_1 l} - e^{-ik_1 l} \right);$$

$$C_1' = G_3' e^{ikl} - G_1'; \; C_2' = -\frac{i G_3'}{k c^T} e^{ikl} + G_2';$$

$$G_1' = E' B_0 \alpha_t \left(\alpha_{eff} \left(\frac{\alpha_{eff} e^{-\alpha_{eff} l}}{\alpha_{eff}^2 + k^2} - \frac{\sigma_S e^{-\sigma_S l}}{\sigma_S^2 + k^2} \right) + \left(\frac{\alpha_{eff}}{\sigma_S} e^{-\sigma_s l} - e^{-\alpha_{eff} l} \right) \right);$$

$$G_2' = E' \frac{B_0 \alpha_t \alpha_{eff}}{c^T} \left(\frac{e^{-\alpha_{eff} l}}{\alpha_{eff}^2 + k^2} - \frac{e^{-\sigma_S l}}{\sigma_S^2 + k^2} \right);$$

$$G_3' = E' B_0 \alpha_t \left(\alpha_{eff} \left(\frac{\alpha_{eff}}{\alpha_{eff}^2 + k^2} - \frac{\sigma_S}{\sigma_S^2 + k^2} \right) + \left(\frac{\alpha_{eff}}{\sigma_S} - 1 \right) \right);$$

$$E' = Q^{TE} \Big/ \left(\alpha_{eff}^2 - \sigma_s^2 \right); \; c^D = c^E \left(1 + e^2 \Big/ \varepsilon^S c^E \right).$$

It is also easy to obtain an expression for the potential difference, taking into account the boundary conditions (10):

$$U^{TE} = \frac{A_1'' C_2'' + A_2'' C_1''}{A_1'' B''_2 - A_2'' B''_1} \left(2e^{-2ik_1 l_1} - e^{-2ik_1 l_1} e^{ik_1 l} - e^{-ik_1 l} \right), \tag{12}$$

where

$$A_2'' = 2i \cos kl; \; A_2'' = 2i \sin kl;$$

$$B_2'' = \left(e^{-2ik_1 l_1} e^{ik_1 l} + e^{-ik_1 l} \right); \; B_1'' = ik_1 c^D \left(e^{-2ik_1 l_1} e^{ik_1 l} - e^{-ik_1 l} \right);$$

$$C_1'' = ik c^T G_3'' e^{ikl} + G_1''; \; G_2'' = G_2',$$

$$C_2'' = -G_3'' e^{ikl} + G_2''; \; G_1'' = G_1';$$

$$G_3'' = E'B_0\alpha_t\alpha_{eff}\left(\frac{1}{\alpha_{eff}^2 + k^2} - \frac{1}{\sigma_S^2 + k^2}\right).$$

Analyzing expressions (11) and (12), we see that the amplitude of the photoacoustic signal is determined in a rather complicated manner and depends on many parameters of the "sample-piezoelectric converter" system. In addition, the magnitude of the resulting signal is significantly affected by the modulating action of Bessel light beams (Figure 5).

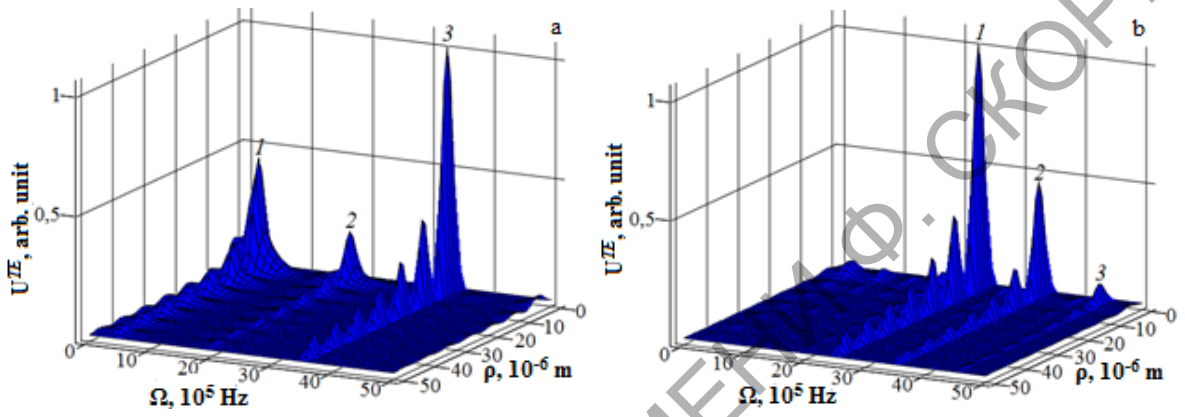

Figure 5 – Dependence of the amplitude of the photoacoustic signal U^{TE} on the radial coordinate when receiving the modulation frequency Ω:
a – the dependence under the boundary conditions (11);
b – dependence under the boundary conditions (12)

As a result of the graphical analysis of expressions (11), (12), a resonant increase in the amplitude was detected.

It should be noted that the amplitude and position of the resonant peaks depend on the type of the boundary conditions imposed on the "sample-piezoelectric converter" system. At the same time, the tendency is generally to decrease the amplitudes of the resonance coordinates, as well as to identify and eliminate inconsistencies.

It can also be seen from the figures that an increase in the cone angle of a BLB affects the frequency of the appearance of resonant peaks as a function of the radial coordinate ρ. Controlling the amplitude of the resulting signal resulting from the modulated absorption of the light beam can be realized by using the taper angle adjustment schemes of the BLBs acting on the basis of the electrochotic Pockels effect [11, 12].

Thus, the model of photoacoustic transformation in the layer of chiral and achiral carbon nanotubes irradiated by the TE-mode of a Bessel light beam is constructed.

References

1.Thermooptical Sound generation by Bessel light beams in nonlinear crystals / G.S. Mityurich [et al.] // International Journal of Thermophysics. –2011. – Vol. 32, № 4. – P. 844–851.

2.Bessel-beam Grueneisen relaxation photoacoustic microscopy with extended depth of field / J. Shi [et al.] // Journal of Biomedical Optics. – 2015. – Vol. 20(11). – p. 116002-1–116002-6.

3. Rapid three-dimensional isotropic imaging of living cells using Bessel beam plane illumination / T.A. Planchon [et al.] // Nature Methods. – 2011. – Vol. 8. – p. 417–423.

4. Multicolor 4D fluorescence microscopy using ultrathin Bessel light sheets / T. Zhao [et al] // Scientific Reports. – 2016. –Vol.6. – p. 26159-1–26159-5.

5.Trivedi, S. Effect of vertically aligned carbon nanotube density on the water flux and salt rejection in desalination membranes / S. Trivedi, K.E. Alameh // SpringerPlus. – 2016. – Vol. 5(1). – p. 1158-1–1158-13.

6. Слепян, Г.Я. Современные тенденции развития наноэлектромагнетизма: аналит. обзор / НИУ «Ин-т ядерных проблем» БГУ; сост. Г.Я. Слепян, С.А. Максименко, П.П. Кужир. – Минск: Изд. центр БГУ, 2012. – 71 с.

7. Митюрич, Г.С. Фотодефлекционный сигнал, генерируемый бесселевым световым пучком в плотном слое углеродных нанотрубок / Г.С. Митюрич, Е.В. Черненок, А.Н. Сердюков. // Проблемы физики, математики и техники. – 2015. – Т. 25, № 4. – С. 20–27.

8. Saito, R. Physical properties of carbon nanotubes / R. Saito, M.S. Dresselhaus, G. Dresselhaus. – London: Imperial College Press, 1999. – 251 p.

9. Mintmire, J.W. Electronic and structural properties of carbon nanotubes / J.W. Mintmire, C.T. White // Carbon. – 1995. – Vol. 33, Iss. 7. – P. 893–902.

10. Mityurich, G.S. Photoacoustic transformation of Bessel light beams in magnetoactive superlattices / G.S. Mityurich, E.V. Chernenok, V.V. Sviridova, A.N. Serdyukov // Crystallography Reports. – 2015. – Vol. 60, № 2. – P. 273–279.

11. Устройство управляемой термооптической генерации акустической волны: пат. 10757u Респ. Беларусь, МПК (2006.01) G10K 11/00 / Г.С. Митюрич, Е.В. Черненок, А.Н. Сердюков; заявитель ГГУ им. Ф. Скорины. – № u 20150083; заявл. 09.09.2015; опубл.

30.09.2015 // Афіцыйны бюл. / Нац. цэнтр інтэлектуал. уласнасці. – 2015. – № 4. – С. 146.

12. Устройство управляемой лазерной генерации звука: пат. 11032u Респ. Беларусь, МПК (2006.01) G10K 11/00 / Г.С. Митюрич, Е.В. Черненок, А.Н. Сердюков; заявитель ГГУ им. Ф. Скорины. – № u 20150378; заявл. 06.11.2015; опубл. 30.04.2016 // Афіцыйны бюл. / Нац. цэнтр інтэлектуал. уласнасці. – 2016. – № 2. – С. 162–163.

Roza Navitskaya, Ihar Stashkevich
Belarusian State University, Minsk, Belarus

DUAL-POLARIZATION GENERATION IN THE ND:YAG LASER

Introduction

Dual-polarization laser generation in dynamic mode is currently used for some interesting applications [1, 2]. We propose using it for passive cavity dumping by the second harmonic generation in the mode locked laser. In this case it is important to have the same radiation intensity at both polarizations.

In this paper, we investigate the effect of the difference between inactive loss coefficients and cavity optical lengths for simultaneously generated polarizations on their intensities.

1. Theoretical model

Dual-polarization generation in dynamic regime is simulated with the use of simple scalar model. The main approximations used in the model are as follows:

a) The pump source (a lamp) produces unpolarized radiation.

b) The *Nd: YAG* active laser medium properties are independent of the optical field polarization: stimulated emission cross-section σ_e and refractive index n of the medium are equal for both polarizations, anisotropic properties of the Nd^{3+} ions are not considered.

c) The cavity anisotropies consist in different coefficients of losses γ and optical cavity lengths L_{opt} for radiation with different polarizations.

Our model may be used to investigate quantitative behavior of the described system, although it may be not enough for more complicated cases. To describe the laser generation in more detaled and correct way, the cor-